Nanoscale

PAPER

View Article Online
View Journal

Cite this: DOI: 10.1039/d5nr04872a

Unravelling the reactions between a hydride-protected Ag_{18} nanocluster and thiol by the crystallization of intermediates

Subrata Duary, [a] Samapti Mondal, [a] Souvik Manna, [b] Soham Chowdhury, [a] Biswarup Pathak *[b] and Thalappil Pradeep *[a]

Received 18th November 2025,
Accepted 20th February 2026

DOI: 10.1039/d5nr04872a

rsc.li/nanoscale

Despite the significant progress accomplished in the synthesis and characterization of atomically precise noble metal nanoclusters (APCs) through ligand exchange-induced structural transformation (LEIST), an in-depth understanding of the chemistry remains elusive. Herein, we report a study of the transformation of $[Ag_{18}H_{16}(TPP)_{10}]^{2+}$ (where H- and TPP are hydride and triphenyl phosphine ligands, respectively) into smaller molecular entities upon ligand exchange with TFMBT-H (acronym for 2,3,5,6-tetrafluoro-4-(trifluoromethyl) benzenethiol) at different stoichiometric ratios, and investigate the reaction pathways using experimental and computational approaches. Different products, namely, $[Ag(TFMBT)(TPP)_3]$, $[Ag_6(TFMBT)_6(TPP)_6]$ and $[Ag_7(TFMBT)_8(TPP)_9]$, were formed depending on the cluster to thiol ratio. The study shows that the composition provides a valuable handle for isolating and characterizing the intermediates involved in the ligand exchange process of clusters.

Introduction

Monolayer-protected atomically precise noble metal nanoclusters (APCs) possessing well-defined compositions and molecule-like electronic structures have gained considerable interest due to their role in deepening the fundamental understanding of nanoscale matter.[1,2] These molecular entities are metastable and transform into other structures triggered by incoming molecules (thiols, phosphines, carbenes, polymers, *etc.*) and external stimuli such as heat, light, surface ligands, pH, *etc.*[3–7] As the structure of APCs largely determines their functions, the transformation of clusters into different structures causes a need to investigate their physicochemical properties in greater detail. Thus, the transformation chemistry of APCs is an interesting area of research, offering new insights into cluster dynamics and reactivity. Ligand-exchange-induced structure transformation (LEIST) of APCs has evolved as a synthesis strategy to introduce new surface-protecting ligands and tune their properties.[5,7,8] Although the LEIST method is well-established, a comprehensive understanding of the structure–property relationship of newly formed nanoclusters during ligand exchange remains elusive. Monitoring the reaction to identify the key intermediates and roles of ligands in the exchange reaction helps to comprehend the nanocluster's structural transformation, growth, and properties. There are some reports on gold clusters describing their transformation and property evolution. Jin *et al.* have revealed the role of structural isomerism in the excited-state dynamics of $Au_{38}(SC_2H_4Ph)_{24}$ nanoclusters.[9] Mandal *et al.* have shown the partial reversible conversion of gold nanoclusters *via* the $Au_{23}(S\text{-}c\text{-}C_6H_{11})_{17}$ intermediate.[10] Yao *et al.* have shown the reversible transformation of a bimetallic AuCd cluster.[11] However, examples of silver nanoclusters remain relatively scarce, likely due to the higher chemical reactivity of the intermediates, a pronounced tendency to aggregate into larger nanoparticles under harsh conditions, and their inherent susceptibility to oxidative degradation.[12–14] This motivated us to investigate the transformation of a silver nanocluster systematically.

In LEIST, the outcome of the reaction is dominated by the incoming thiol. It plays an important role in determining the core size and structure of newly formed products through its steric demand, coordination preference and electronic characteristics.[15–17] It manipulates properties (optical/electronic) through its electron push–pull effect.[18] Sometimes, different non-covalent interactions (CH–π, π–π, *etc.*) of protected ligands in the solid state enhance emission by promoting radiative decays.[15a,b]

Herein, we have conducted an investigation of the reaction of $[Ag_{18}H_{16}(TPP)_{10}]^{2+}$ (briefly, Ag_{18}) with 2,3,5,6-tetrafluoro-4-(trifluoromethyl)benzenethiol (briefly, TFMBT-H) at stoichiometric ratios of 1 : 1, 1 : 2 and 2 : 1, respectively. For a cluster to thiol ratio of 1 : 1, the disintegration of Ag_{18} leads to several

[a]DST Unit of Nanoscience (DST UNS) and Thematic Unit of Excellence (TUE), Department of Chemistry, Indian Institute of Technology Madras, Chennai 600036, India. E-mail: pradeep@iitm.ac.in
[b]Department of Chemistry, Indian Institute of Technology Indore, Indore 453552, India. E-mail: biswarup@iiti.ac.in

smaller species as products, proceeding through a visible colour change of the reaction solution during the course of the reaction. Two stable intermediates were crystallized from the initial and final reaction mixtures, namely, $[Ag(TFMBT)(TPP)_3]$ and $[Ag_6(TFMBT)_6(TPP)_6]$ (briefly Ag-1 and Ag-6, respectively). For a 1 : 2 ratio, Ag_{18} produces small complexes with the reaction solution becoming a stable white suspension. Whereas, Ag_{18} transforms into $[Ag_7(TFMBT)_8(TPP)_9]$ (briefly, Ag-7) with stable brown coloured solution for 2 : 1 ratio.

Results and discussion

The precursor cluster Ag_{18} was synthesized by a direct reduction method following a reported procedure (see the Experimental section in the SI).[19] The Ag_{18} nanocluster was characterized using UV-vis spectroscopy, electrospray ionization mass spectrometry (ESI MS) and transmission electron microscopy (TEM) (Fig. S1). The cluster core is composed of silver–hydride (Ag–H) bonds, which are labile. When thiol (TFMBT-H) is added, its core disintegrates, which is likely due to the formation of covalent Ag–S bonds, resulting from orbital overlap between silver and sulphur.[20] Transformation of the Ag_{18} nanocluster was performed upon probing it with different stoichiometric ratios of the cluster to thiol (1 : 1, 1 : 2 and 2 : 1) under ambient conditions. For a cluster to thiol ratio of 1 : 1, the transformation was monitored through UV-vis spectroscopy, TEM and ESI MS. The Ag_{18} nanocluster dissolved in methanol shows UV-vis peaks at 554 and 618 nm, which vanished immediately after the addition of thiol (Fig. 1a). UV-vis spectra of the reaction mixture (10 μL diluted to 1.5 mL methanol) show two prominent peaks at 430 and 490 nm, and a small broad peak at 770 nm. With the progress of the reaction, the 770 nm peak disappeared, while the other two peaks

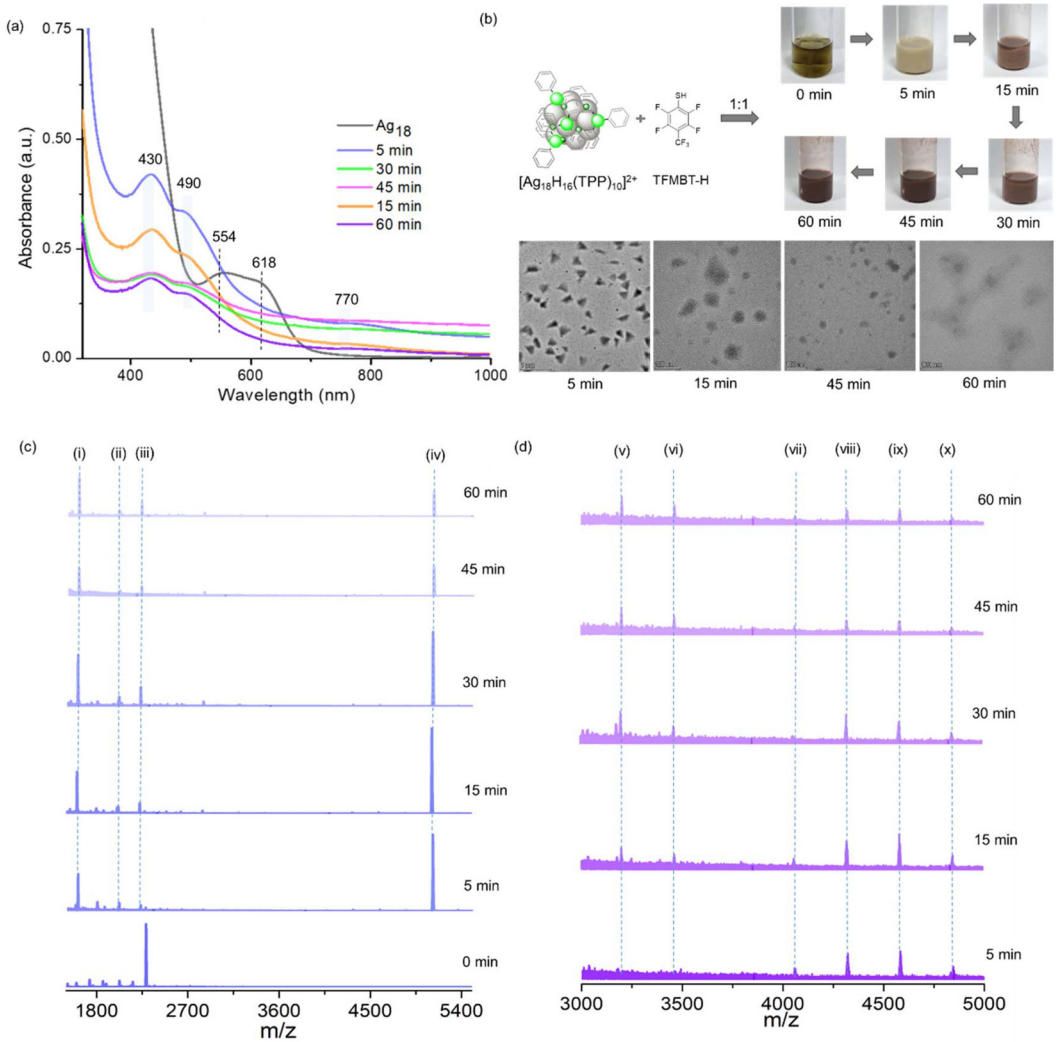

Fig. 1 Reaction monitoring of ligand exchange for a cluster to thiol ratio of 1 : 1. (a) Time dependent UV-vis spectra showing the Ag_{18} nanocluster's transformation; the rise in the background from 5 min is due to the turbidity of the solution. (b) Scheme of the reaction and photographs of visible colour change at different times. Inset: TEM images (below panel) showing aggregate-mediated cluster transformation (scale bars: 1 μm and 100 nm, respectively). (c and d) ESI MS spectra indicating the formation of the intermediates with the progress of the reaction.

remain prominent. After 5 min of reaction, a white suspension (inset of Fig. 1b) with yellow emission was formed, which gradually changed to a brown coloured solution with quenched emission (Fig. S2). Such a visible colour change of the cluster solution (photographs of Fig. 1b) and changes in UV-vis spectra (Fig. 1a) indicate that the transformation of Ag_{18} occurs in a stepwise manner. The reaction was monitored up to 60 min, presenting the changes in the absorption characteristics of *in situ* formed species (Fig. 1a). TEM images show that the Ag_{18} nanocluster forms aggregates upon reaction with thiol (lower panel of Fig. 1b, 5 min), which exhibit yellow emission (Fig. S2a). Such aggregates become smaller with time (lower panel of Fig. 1b, 60 min). This type of aggregate-induced cluster growth and size focusing is similar to the seed-mediated or nanoparticle-mediated growth of noble metal nanoclusters.[21] To understand the molecular transformation during the reaction, *in situ* formed species were analyzed using high-resolution ESI MS at different time intervals (Fig. 1c and d, ionization conditions are provided in the Experimental section of the SI). Full range ESI MS spectra are presented in Fig. 1c, and an expanded region is presented in Fig. 1d. It reveals that the peak at *m*/*z* 2290.16 (2+) corres-

Table 1 List of molecular species for a 1 : 1 reaction between the cluster and thiol

Molecular species	*m*/*z*	Molecular formula
i	1608.72	$Ag_3(TFMBT)_2(TPP)_3$
ii	2228.02	$Ag_4(TFMBT)_3(TPP)_4$
iii	2847.31	$Ag_5(TFMBT)_4(TPP)_5$
iv	5108.02	$Ag_7(TFMBT)_8(TPP)_9$
v	3204.30	$Ag_6(TFMBT)_5(TPP)_5$
vi	3466.59	$Ag_6(TFMBT)_5(TPP)_6$
vii	4058.11	$Ag_7(TFMBT)_8(TPP)_5$
viii	4321.20	$Ag_7(TFMBT)_8(TPP)_6$
ix	4583.91	$Ag_7(TFMBT)_8(TPP)_7$
x	4844.11	$Ag_7(TFMBT)_8(TPP)_8$

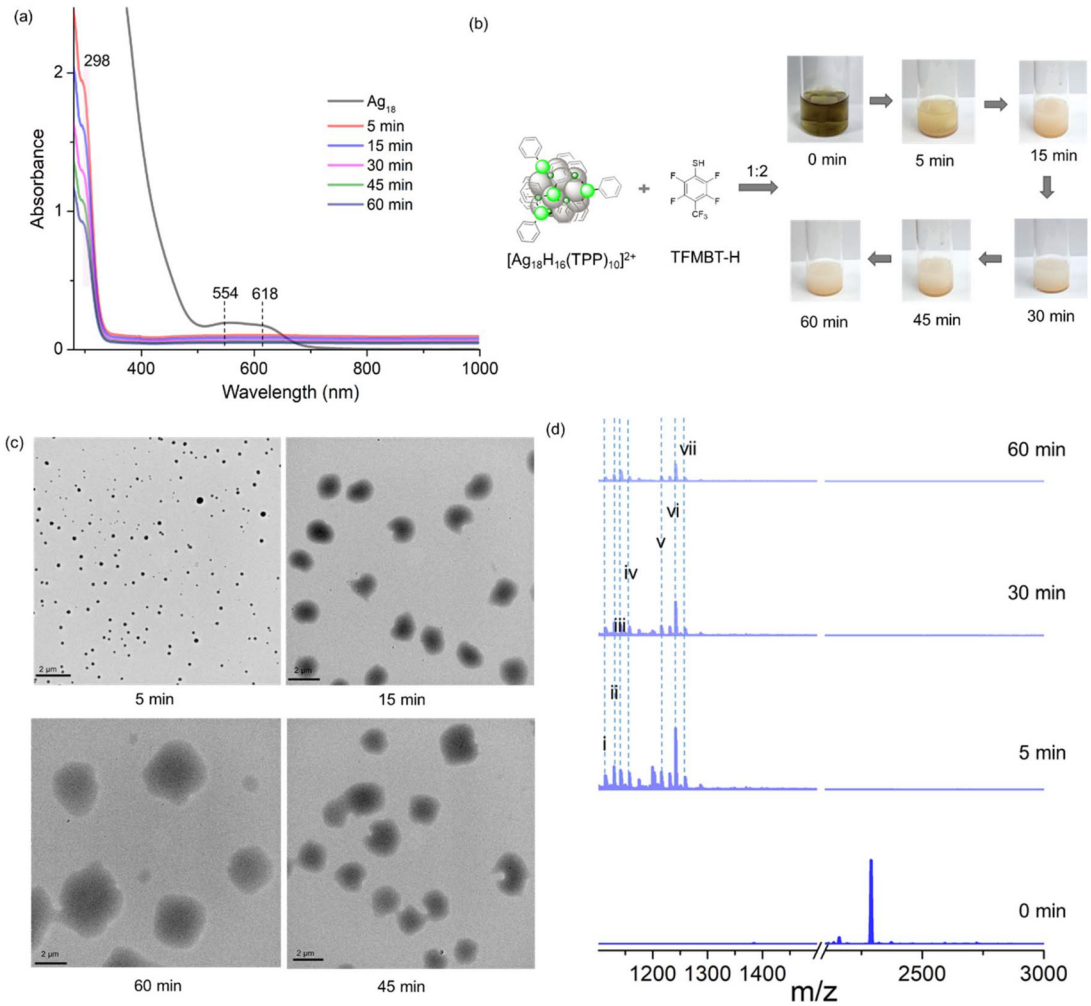

Fig. 2 Reaction monitoring of ligand exchange for a cluster to thiol ratios of 1 : 2. (a) Time dependent UV-vis spectra showing the Ag_{18} nanocluster's transformation. (b) Scheme of the reaction and photographs of the reaction mixture showing that the colour of the mixture remains white during the course of the reaction. (c) TEM images at different times show aggregates (scale bar: 2 μm). (d) ESI MS spectra indicate the formation of small complexes during the course of the reaction.

Table 2 List of molecular species for a 1 : 2 reaction between the cluster and thiol

Molecular species	*m*/*z*	Molecular formula
i	1117.21	$Ag(TFMBT)_3(TPP)$
ii	1130.12	$Ag(TFMBT)_2(TPP)_2$
iii	1143.56	$Ag(TFMBT)(TPP)_3$
iv	1156.31	$Ag(TPP)_4$
v	1212.12	$Ag_2(TFMBT)_4$
vi	1237.42	$Ag_2(TFMBT)_2(TPP)_2$
vii	1252.08	$Ag_2(TFMBT)(TPP)_3$

ponding to the Ag_{18} nanocluster disappeared immediately, and it formed a mixture of different nuclearities; Ag_7, Ag_6, Ag_5, Ag_4 and Ag_3 (i–x, the insets of Fig. 1c and d). The composition of the *in situ* formed molecular species is presented in Table 1. Matching between the isotopic mass distributions of the experimental and simulated spectra is shown in Fig. S4. Surprisingly, the Ag_6 cluster's peaks (*m*/*z* 3204.30 and 3466.59) increased gradually with time (15 min to 60 min) and remained prominent (Fig. 1d), which suggests its growing concentration in solution before its subsequent isolation through crystallization. Next, we have studied the reaction using cluster to thiol ratios of 1 : 2 and 2 : 1 sequentially. For the stoichiometric ratio of 1 : 2, immediate formation of a white suspen-

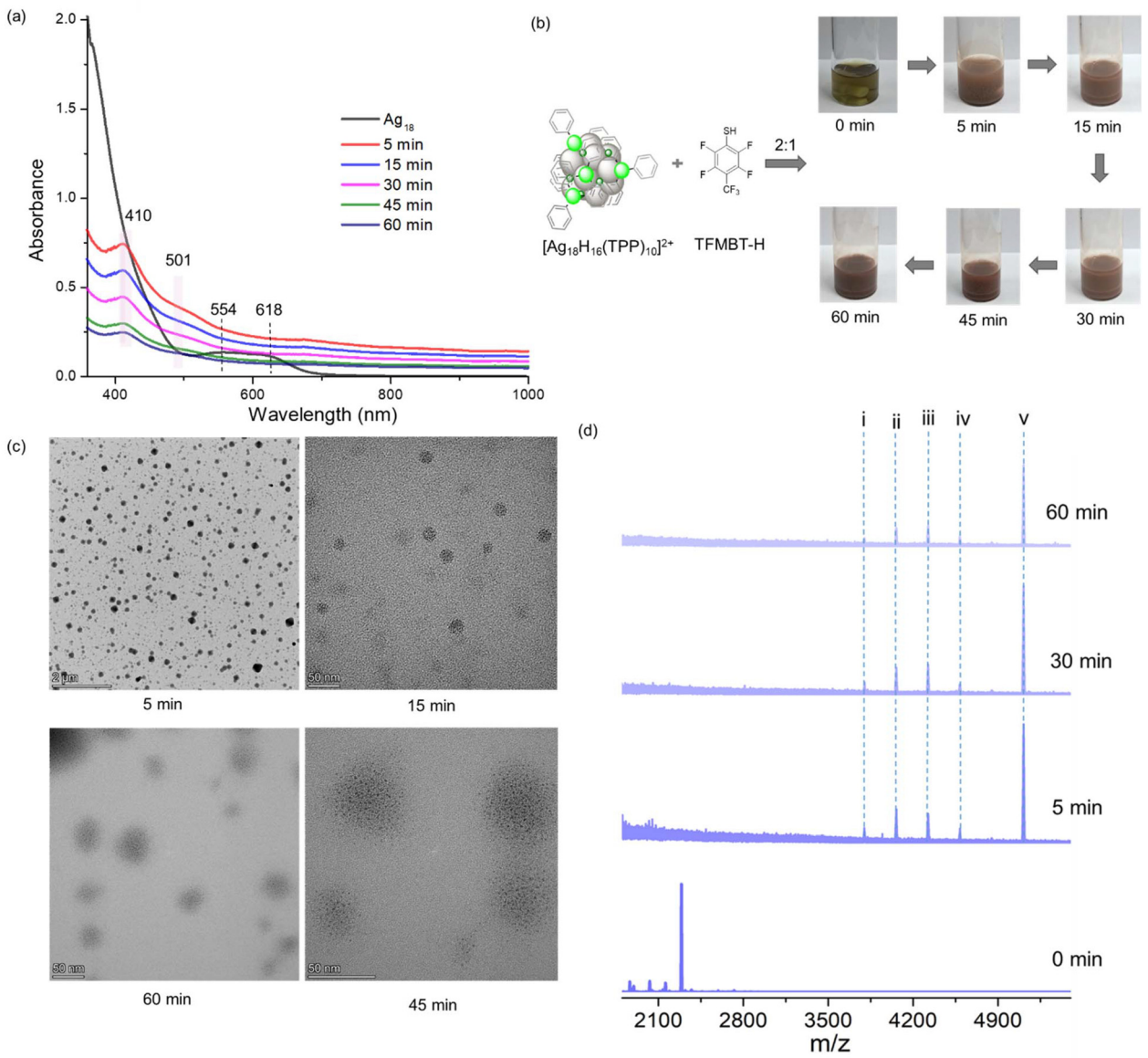

Fig. 3 Reaction monitoring of ligand exchange for a cluster and thiol ratio of 2 : 1. (a) Time dependent UV-vis spectra showing Ag_{18} nanocluster's transformation. (b) Scheme of the reaction and photographs of reaction solution showing that the colour of the reaction mixture remains brown during the course of the reaction. (c) TEM images at different times show aggregates of clusters (scale bars: 2 μm and 50 nm, respectively). (d) ESI MS spectra indicate the formation of Ag-7 exclusively.

sion was observed, and the solution colour remains the same over time (upper panel of Fig. 2b). UV-vis spectra show one peak at 298 nm (Fig. 2a). TEM images show the formation of larger aggregates in solution (Fig. 2c). Time dependent ESI MS spectra show that the parent peak (2290.16, 2+) of Ag_{18} immediately vanished, and small nuclearity complexes were produced (Fig. 2d). The composition of these complexes is presented in Table 2. For the stoichiometric ratio of 2 : 1, the solution colour becomes brown after adding thiol to it, and its colour remains the same over time (upper panel of Fig. 3b). UV-vis spectra show two peaks at 410 and 501 nm, which become less intense with time. TEM images indicate the agglomeration of clusters with time (lower panel of Fig. 3d). Time dependent ESI MS spectra show that Ag-7 was formed as a major product (Fig. 3c). Due to phosphine (PPh_3) loss from Ag-7 species, other peaks were also observed. The composition corresponding to such peaks is presented in Table 3.

Crystallization of the stable intermediate species was carried out for different stoichiometric ratios of cluster to thiol (scheme described in Fig. S5). For the 1 : 1 reaction, two intermediate species, namely, $[Ag(TFMBT)(TPP)_3]$ and $[Ag_6(TFMBT)_6(TPP)_6]$ (briefly, Ag-1 and Ag-6), were crystallized from the white cloudy suspension (reaction mixture, 5 min) by hexane diffusion at 4 °C, and from the brown solution (reaction mixture, 45 min) in a mixed solvent of MeOH–$CHCl_3$, respectively. Ag-1 was also crystallized from a white suspension of the 1 : 2 reaction mixture, but no crystal was grown from the 2 : 1 reaction mixture. UV-vis spectra reveal that Ag-1, Ag-6 and Ag-7 are stable for ~6 days, ~15 days and ~10 days, respectively (Fig. S6). Field emission scanning electron microscopy (FESEM) of single crystals of Ag-1 and Ag-6 verifies the different elemental compositions (Fig. S7). The powder X-ray diffraction spectrum of the synthesized Ag-1 and Ag-6 was recorded using ~25 mg of the microcrystalline sample, and it shows similar peaks as predicted from single crystal structure analysis (Fig. S21). Ag-1 belongs to the triclinic crystal system with the $P\bar{1}$ space group. In the solid state packing, Ag-1 molecules are arranged in a linear chain as revealed by SC-XRD analysis (Fig. 4a). Two molecules of Ag-1 are present in each unit cell, and silver is coordinated by three phosphorus and one sulphur donor site of ligands (Fig. S8a and S8c). In the solid state, Ag-1 molecules are held together by different supramolecular interactions like CH–π, CH–F, and CF–π (Fig. S8a). Such non covalent interactions restrict intermolecular rotations and vibrations, and thus promote radiative transitions in the solid state, making Ag-1 yellow emissive (emission ~550 nm, Fig. S18).[23] Ag-6 belongs to the trigonal crystal system with the $R\bar{3}$:H space group. In the solid state packing, Ag-6 molecules are arranged in a linear channel, as revealed by SC-XRD analysis (Fig. 4b). Three molecules of Ag-6 are present per unit cell, and each silver is coordinated by three μ_3-sulphur and

Table 3 List of molecular species for a 2 : 1 reaction between the cluster and thiol

Molecular species	m/z	Molecular formula
i	3796.74	$Ag_7(TFMBT)_8(TPP)_4$
ii	4059.22	$Ag_7(TFMBT)_8(TPP)_5$
iii	4321.35	$Ag_7(TFMBT)_8(TPP)_6$
iv	4583.61	$Ag_7(TFMBT)_8(TPP)_7$
v	5108.08	$Ag_7(TFMBT)_8(TPP)_9$

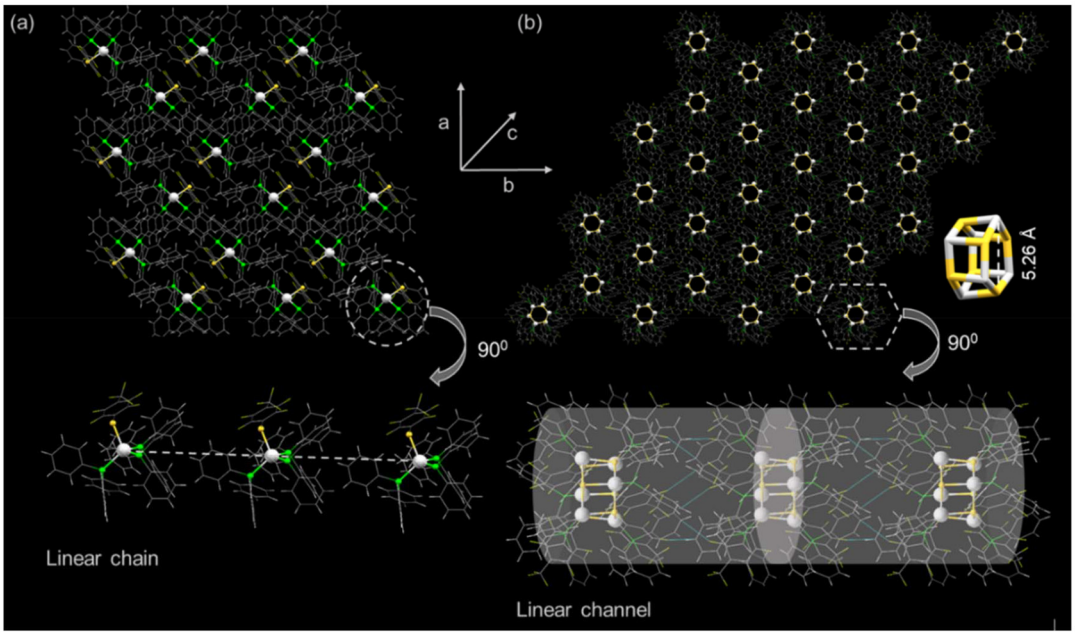

Fig. 4 Single crystal structure and packing along the c-axis. (a) Structured packing (3 × 3 × 3) of Ag-1 showing a chain-like orientation. (b) Structured packing (3 × 3 × 3) of Ag-6 showing a channel-like orientation with a pore size of 5.26 Å. Channel and pores are clearly visible along the b-axis.

one phosphorus donor site (Fig. S8b and S8d). The sequential arrangement of Ag and S leads to a stable Ag_6S_6 cyclic porous framework with a diameter of ~5.26 Å. Ag_6S_6 molecules are held together through CF–π interactions of their ligand shells (Fig. 4b). X-ray photoelectron spectroscopy (XPS) analysis shows the presence of all elements in the respective crystal structures of Ag-1 and Ag-6 (Fig. S9). The binding energies of Ag $3d_{5/2}$ in Ag-1 and Ag-6 are 368.4 and 368.3 eV, respectively (inset of Fig. S9a and b). The Ag MNN Auger spectrum of Ag-1 shows peaks at kinetic energies of 349.4 and 354.6 eV, respectively, which indicates silver (+1) (Fig. S10a). For Ag-6, the peaks are at 351.6 and 356.8 eV, respectively, which indicates that the oxidation state of silver lies in-between 0 and +1 (Fig. S10b). The binding energies of S $2p_{1/2}$ in Ag-1 and Ag-6 are 163.6 and 163.8 eV, respectively (inset of Fig. S9a and b). To understand the electronic energy levels and the associated optical properties of Ag-1 and Ag-6, their structures were optimized using density functional theory (DFT) with the Gaussian 09 package,[22] and the optimized structures are shown in Fig. S11. Further computational details are provided in the SI. The time dependent DFT calculations of Ag-1 reveal that the experimental absorption peaks of Ag-1 at 260 nm and 273 nm correspond to transitions involved in HOMO−3 → LUMO+24 (4.84 eV/256 nm) and HOMO−1 → LUMO+17 (4.47 eV/277 nm), respectively (Fig. S12). The Kohn–Sham (K–S) molecular orbital (MO) analysis shows that the occupied MOs are dominated by S (3p), P (3p), C (2p), and Ag (4d) orbitals in the optical transitions (Fig. S13). In contrast, unoccupied MOs are dominated by Ag (5s) and C (2p) orbitals. Projected density of states (PDOS) analysis shows that the band gaps of Ag-1 derived from the SC-XRD and DFT-optimized structure are 2.80 and 2.30 eV, respectively (Fig. S14). TD-DFT calculations of Ag-6 reveal that the experimental absorption peaks at 413 nm and 496 nm correspond to the electronic transitions involved in HOMO−7 → LUMO+2 (3.37 eV/410 nm) and HOMO−2 → LUMO+1 (2.55 eV/486 nm), respectively (Fig. S15). These transitions shown in occupied MOs are dominated by S (3p), Ag (4d), and C (2p) orbitals, whereas the unoccupied MOs are dominated mainly by C (2p) and Ag (5s), as depicted in Fig. S16. PDOS analysis shows that the band gaps of Ag-6 derived from the SC-XRD and DFT-optimized structures are 2.70 and 2.50 eV, respectively (Fig. S17).

Conclusions

This study presents a systematic investigation of the transformation of the $[Ag_{18}H_{16}(TPP)_{10}]^{2+}$ (Ag_{18}) nanocluster upon stoichiometric reaction with 2,3,5,6-tetrafluoro-4-(trifluoromethyl)benzenethiol (TFMBT-H) using UV-vis, TEM, and ESI MS results together. For a cluster to thiol ratio of 1 : 1, Ag_{18} disintegrates into several smaller species proceeding through a visible colour change of the reaction solution. Two intermediates, $[Ag(TFMBT)(TPP)_3]$ and $[Ag_6(TFMBT)_6(TPP)_6]$ (Ag-1 and Ag-6, respectively), were crystallized from a yellow emissive white suspension and a non-emissive brown solution. For the cluster to thiol ratios of 1 : 2 and 2 : 1, Ag_{18} cluster transforms into a yellow-emissive white suspension and a non-emissive brown solution, respectively, which are predominantly populated with small complexes and the Ag-7 cluster, as revealed by ESI-MS. This study indicates that the stoichiometric ratio of cluster to thiol emerges as a valuable handle for controlling the transformation of the Ag_{18} nanocluster into smaller molecular entities. Overall, this work presents an understanding of an atomically precise metal nanocluster's transformation by capturing the intermediates.

Author contributions

S. D. performed the synthesis, characterization, photoluminescence studies, and data interpretation. S. M. helped by measuring the ESI MS of clusters. S. M. and B. P. performed the theoretical calculations. S. C. helped in measuring the XPS. The draft of the manuscript was written by S. D. T. P. supervised the work and refined the manuscript.

Conflicts of interest

The authors declare no conflict of interest.

Data availability

Data supporting this article have been presented in the supplementary information (SI). Supplementary information: a brief discussion of the experimental protocol, crystallographic details, computations, and other physical measurements. See DOI: https://doi.org/10.1039/d5nr04872a.

CCDC 2497804 and 2497805 contain the supplementary crystallographic data for this paper.[24a,b]

Acknowledgements

S. D. acknowledges the Prime Minister's Research Fellowship (PMRF) from the Government of India (GoI). S. D. thanks Dr Sudhadevi Antharjanam and Sophisticated Analytical Instrumental Facility, Indian Institute of Technology Madras (SAIF-IITM), for the single crystal XRD data. T. P. acknowledges funding from the Centre of Excellence (CoE) on Molecular Materials and Functions from the Institute of Eminence Scheme of IIT Madras. He also thanks the Science and Engineering Research Board (SERB), India, for funding through a research grant (SPR/2021/000439) and a JC Bose Fellowship. TEM measurements were collected at the ANRF National Facility for Cryo-Electron Microscopy at IIT Madras.

References

1 I. Chakraborty and T. Pradeep, *Chem. Rev.*, 2017, **117**, 8208–8271.

2 R. Jin, C. Zeng, M. Zhou and Y. Chen, *Chem. Rev.*, 2016, **116**, 10346–10413.
3 R. Jin, E. Shunji and N. F. Scherer, *J. Am. Chem. Soc.*, 2004, **126**, 9900–9901.
4 (*a*) A. Jana, M. Jash, A. K. Poonia, G. Paramasivam, Md. R. Islam, P. Chakraborty, S. Antharjanam, J. Machacek, S. Ghosh, K. N. V. D. Adarsh, T. Base and T. Pradeep, *ACS Nano*, 2021, **15**, 15781–15793; (*b*) R. Gupta, S. Agrawal, S. Rai, J. Sarkar, S. Kumari, D. Shil and S. Mukherjee, *ACS Appl. Opt. Mater.*, 2024, **2**, 1880–1890; (*c*) H. Kawasaki, K. Hamaguchi, I. Osaka and R. Arakawa, *Adv. Funct. Mater.*, 2011, **21**, 3508–3515.
5 X. Kang and M. Zhu, *Chem. Mater.*, 2019, **31**, 9939–9969.
6 (*a*) L. G. AbdulHalim, Z. Hooshmand, M. R. Parida, S. M. Aly, D. Le, X. Zhang, T. S. Rahman, M. Pelton, Y. Losovyj, P. A. Dowben and O. M. Bakr, *Inorg. Chem.*, 2016, **55**, 11522–11528; (*b*) H. Tsunoyama, H. Sakurai, Y. Negishi and T. Tsukuda, *J. Am. Chem. Soc.*, 2005, **127**, 9374–9375.
7 X. Zou, K. Xi and M. Zhu, *Chem. Soc. Rev.*, 2023, **52**, 5892–5967.
8 Q. Yao, Z. Wu, Z. Liu, Y. Lin, X. Yuan and J. Xie, *Chem. Sci.*, 2021, **12**, 99–127.
9 M. Zhou, S. Tian, C. Zeng, M. Y. Sfeir, Z. Wu and R. Jin, *J. Phys. Chem. C*, 2017, **121**, 10686–10693.
10 S. Gratious, E. Mahal, J. Thomas, S. Saha, A. S. Nair, K. V. Adarsh, B. Pathak and S. Mandal, *Chem. Sci.*, 2024, **15**, 9823–9829.
11 H. Xiang, H. Yan, J. Liu, R. Cheng, C. Q. Xu, J. Li and C. Yao, *J. Am. Chem. Soc.*, 2022, **144**, 14248–14257.
12 J. Yang and R. Jin, *ACS Mater. Lett.*, 2019, **1**, 482–489.
13 Y. Jin, C. Zhang, X. Y. Dong, S. Q. Zang and T. C. Mak, *Chem. Soc. Rev.*, 2021, **50**, 2297–2319.
14 F. Tian and R. Chen, *J. Am. Chem. Soc.*, 2019, **141**, 7107–7114.
15 (*a*) S. Duary, A. Jana, A. Das, S. Acharya, A. R. Kini, J. Roy, A. K. Poonia, D. K. Patel, V. Yadav, P. S. Antharjanam, B. Pathak, K. N. V. D. Adarsh and T. Pradeep, *Inorg. Chem.*, 2024, **63**, 18727–18737; (*b*) S. Duary, A. Jana, A. Das, A. Sharma, B. Pathak, K. N. V. D. Adarsh and T. Pradeep, *Inorg. Chem.*, 2025, **64**, 11001–11011; (*c*) A. Jana, S. Duary, A. Das, A. R. Kini, S. Acharya, J. Machacek, B. Pathakand and T. Pradeep, *Chem. Sci.*, 2024, **15**, 13741–13752.
16 (*a*) A. Jana, P. M. Unnikrishnan, A. K. Poonia, J. Roy, M. Jash, G. Paramasivam, J. Machacek, K. N. V. D. Adarsh, T. Base and T. Pradeep, *Inorg. Chem.*, 2022, **61**, 8593–8603; (*b*) M. S. Bootharaju, V. M. Burlakov, T. M. Besong, C. P. Joshi, L. G. AbdulHalim, D. M. Black, R. L. Whetten, A. Goriely and O. M. Bakr, *Chem. Mater.*, 2015, **27**, 4289–4297; (*c*) T. Ubayasena, B. Bhattarai, B. Yoon, U. Landman and T. P. Bigioni, *J. Phys. Chem. C*, 2024, **129**, 878–888.
17 (*a*) Y. Wang and T. Bürgi, *Nanoscale Adv.*, 2021, **3**(10), 2710–2727; (*b*) L. O. Brown and J. E. Hutchison, *J. Am. Chem. Soc.*, 1997, **119**, 12384–12385; (*c*) R. Guo, Y. Song, G. Wang and R. W. Murray, *J. Am. Chem. Soc.*, 2005, **127**, 2752–2757.
18 T. M. Carducci, R. E. Blackwell and R. W. Murray, *J. Phys. Chem. Lett.*, 2015, **6**, 1299–1302.
19 M. S. Bootharaju, R. Dey, L. E. Gevers, M. N. Hedhili, J. M. Basset and O. M. Bakr, *J. Am. Chem. Soc.*, 2016, **138**, 13770–13773.
20 A. F. Pedicini, A. C. Reber and S. N. Khanna, *J. Chem. Phys.*, 2013, **139**, 164317.
21 (*a*) Q. Yao, X. Yuan, V. Fung, Y. Yu, D. T. Leong, D.-E. Jiang and J. Xie, *Nat. Commun.*, 2017, **8**, 927–937; (*b*) L. Qiao, N. Pollard, R. D. Senanayake, Z. Yang, M. Kim, A. S. Ali, M. T. Hoang, N. Yao, Y. Han, R. Hernandez, A. Z. Clayborne and M. R. Jones, *Nat. Commun.*, 2023, **14**, 4408; (*c*) P. Mahato, K. Mandal, K. Paria, D. Chopra and S. Mukherjee, *Angew. Chem.*, 2024, **136**, 202409141.
22 N. Phaisangittisakul, K. Paiboon, T. Bovornratanaraks and U. Pinsook, *J. Nanopart. Res.*, 2012, **14**, 1–10.
23 (*a*) Z. Han, X. Y. Dong, P. Luo, S. Li, Z. Y. Wang, S. Q. Zang and T. C. Mak, *Sci. Adv.*, 2020, **6**, 0107; (*b*) T. Q. Yang, B. Peng, B. Q. Shan, Y. X. Zong, J. G. Jiang, P. Wu and K. Zhang, *Nanomaterials*, 2020, **10**, 261.
24 (*a*) CCDC 2497804: Experimental Crystal Structure Determination, 2026, DOI: 10.5517/ccdc.csd.cc2pv5b2; (*b*) CCDC 2497805: Experimental Crystal Structure Determination, 2026, DOI: 10.5517/ccdc.csd.cc2pv5c3.